# Characterization of surface primary roughness: application to large scale rock joint morphology


Tikou Belem
*Department of Applied Sciences – Université du Québec UQAT, Rouyn-Noranda, Quebec, Canada*

ABSTRACT
In this paper numerous quantitative parameters have been proposed for the characterization of the primary roughness of rock joint surface. Indeed, the primary roughness is the only component that prevails during large-slip faults of more than 50 m. The proposed parameters include: the degrees of apparent and real structural anisotropy of surface, the coefficients of real anisotropy and geometrical irregularity, the anisotropy function and the degree of waviness. The formulation of the parameters allows their application at both lab and field scales.

RÉSUMÉ
Dans cet article, de nombreux paramètres quantitatifs ont été proposés pour la caractérisation de la rugosité primaire des surfaces des joints rocheux. En effet, la rugosité primaire est la seule composante qui prévaut lors des grands glissements de failles pouvant dépasser 50 m. Les paramètres proposés sont: les degrés d'anisotropie structurale apparente et réelle de la surface, les coefficients d'anisotropie réelle et d'irrégularité géométrique, la fonction d'anisotropie et le degré d'ondularité. La formulation des paramètres permet leur application à la fois au laboratoire et à l'échelle du terrain.

## 1 INTRODUCTION

On sheared laboratory rock joint samples, it was observed that the effective contact area is only a small portion of the total area. The shape of damaged areas depends on the texture of the fracture surface, including asperity size and shape, and the mechanical properties of the rock material, shear direction, normal stress, and shear displacement (Grasselli 2006). Joint roughness undergoes continuous changes with shearing due to wearing, grinding, breaking and crushing of asperities (Belem et al. 2007).

In the literature, most of the experimental studies for modeling the mechanical behavior of rock joints are carried out on various types of artificial joints (rocks and mortars). The morphology of these joints has been in saw teeth, irregular triangles, a combination of various triangles, undulations, etc. But a closer look shows that the common point between these surfaces is their anisotropy (Belem et al. 2000, Belem et al. 2007). Indeed, all these surfaces present distinct structures (or characteristics) along $x$ and $y$ directions (regular or irregular geometry) which will involve necessarily a different mechanical behavior according to $x$ (0° or 180°) and $y$ (90° or 270°) directions (Grasselli 2006). It can be anticipated that a single parameter does not sufficiently characterize the roughness which includes such morphological characteristics as magnitude (surface point elevations), angularity and geometric texture (asperity slopes and angles), waviness (periodicity), anisotropy, and, in a less pronounced way, curvature (Belem et al. 2000).

It is common practice to obtain rock fracture properties by performing laboratory testing on samples of smaller fractures having limited size (e.g., 100–400 mm). This may or may not be a sufficient size to reach the "stationarity threshold" of even the smaller fractures, as surface roughness is scale dependant (Rasouli and Harrison 2000, Fardin et al. 2001, Fardin 2008, Sharifzadeh et al. 2008). According to Jing (2003), there is an acute lack of understanding of the hydro-mechanical behavior of large fractures (such as faults and fracture zones) with a large width (e.g., 10 mm–50 m). Consequently, there is a lack of proper constitutive models for large fracture zones, which in turn reduces our current capacity to develop numerical models for large-scale problems (Jing 2003). There is usually uncertainty concerning scaling experimental results to field application (use of empirical methods).

As an alternative, new laser-based 3D high resolution scanners have recently been developed to measure large-scale fracture surface roughness over scales of 10 µm to 120 m (Feng et al. 2003, Renard et al. 2006, Sagy et al. 2007, Lato et al. 2007 and 2009). Exposed fault surface data provided the first quantitative evidence that fault-surface roughness evolves with increasing slip. It has been observed that small-slip faults (slip < 1 m) are rougher than large-slip faults (slip 10–100 m or more) parallel to the slip direction (Sagy et al. 2007). These authors also observed that surfaces of small-slip faults have asperities over the entire range of observed scales, while large-slip fault surfaces are polished at small scale but have undulating structure at scales of a few to several meters. Thus, at scales of 1–2 m parallel to the slip, the roughness of large-slip faults is about one order of magnitude smoother than that of small-slip faults.

These observations have at least two implications: i) both joint surface primary (waviness) and secondary (asperities) roughness components must be taken into account in modeling sliding or shearing distances up to 1

m. Indeed, a relationship was observed by Sagy et al. (2007) between laboratory and field data for small-slip faults (slip < 1 m), since the power spectra measured by the lab profilometer and field LiDAR (Light detection and ranging) follow a similar trend (continuity). This continuity across five orders of magnitude demonstrates at the same time the consistency of the two different measurement tools; ii) over shearing distances up to 10 m, only surface primary roughness prevails (waviness), and must be taken into account in joint characterization. At this large scale, the power spectra measured by the lab profilometer and field LiDAR for large-slip faults do not connect across scales (Sagy et al. 2007). The joint morphology can be subdivided into two main components (Kana et al. 1996): the secondary or second-order roughness (asperities component) and the primary or first-order roughness (waviness component). The asperities are defined by the surface heights distribution (which correspond to the *sensu stricto* roughness) while the primary roughness is defined by the overall surface texture geometry (which describe the surface anisotropy). Figure 1 is an illustration of the two different components of surface texture (asperities and waviness).

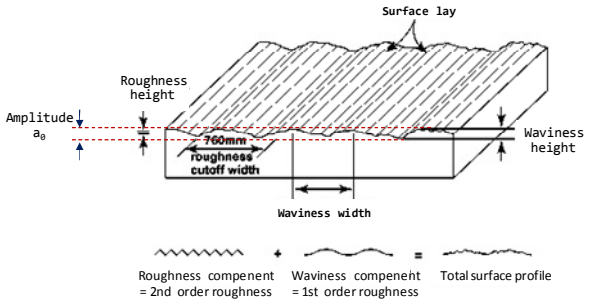


Figure 1. Joint surface morphology waviness (1st order) and asperities (2nd order) components (adapted from Tarr)

The main objective of the research is to characterize rock joint surface primary roughness through quantitative parameters. Primary roughness includes surface amplitude and angularity that can be characterized based on surface 3D profilometric data. Also, the primary roughness is characterized in terms of real and apparent structural anisotropy, geometric irregularity and waviness of surface.

## 2 PREVIOUS WORKS

The real structural anisotropy of a rock joint surface is characterized by means of geostatistical analysis (semi-variogram and auto-correlation function), while the apparent anisotropy is characterized with the aid of directional angularity parameters calculated along both horizontal (*x*-axis, 0°/180° direction) and transverse (*y*-axis, 90°/270° direction) axes (Belem et al. 2000). The geometric irregularity is quantified using the positive and negative angularity parameters. For this purpose, it was assumed that the fracture surface satisfies the second order stationary condition and consequently, the surface asperity heights must be measured with respect to its mean plane (data detrending).

### 2.1 Background on geostatistical analysis

In geostatistical sense a regionalized (spatial) phenomenon is known as anisotropic if it presents particular directions of variability. But these privileged directions must correspond to genetic phenomena known *a priori* (Journel 1975). The structural analysis of the 1D semi-variograms in all directions can reveal three types of behavior: i) isotropic variability where the semi-variograms have the same "range" value as well as the same "sill", ii) proportional effect where the semi-variograms have the same sill but different variances and iii) anisotropic variability where the semi-variograms present the same global variability, in particular the same sill but with different "range" values.

The variographic analysis showed that the "range" value $a_i$ of the variogram and the correlation distance $d_c$ of the correlogram quantify the influence zone limit of the analysed structure. Consequently, knowing the values of $a_i$ and $d_c$ in all directions allows characterizing the real structural anisotropy of the rock joint surfaces. Rather than calculating directional 1D semi-variograms or 1D correlograms, it is preferable to obtain a map representation (iso-value contours) of the incremental variances $\gamma^*$ (2D variogram or "variomap", Eq.1) and the correlations $\rho$ (2D auto-correlograms or "auto-correlomap", Eq.2) using the following relationships:

$$\gamma^*(h_x,h_y)=\frac{1}{2\left[(M-h_x)(N-h_y)\right]}\sum_{j=1}^{M-h_x}\sum_{k=1}^{N-h_y}\left(Z_{j+h_x,k+h_y}-Z_{j,k}\right)^2 \quad [1]$$

$$\rho(h_x,h_y)=\frac{\frac{1}{(M-h_x)(N-h_y)}\sum_{j=1}^{M-h_x}\sum_{k=1}^{N-h_y}\left(Z_{j,k}-\bar{Z}\right)\left(Z_{j+h_x,k+h_y}-\bar{Z}\right)}{\frac{1}{MN}\sum_{j=1}^{M}\sum_{k=1}^{N}\left(Z_{j,k}-\bar{Z}\right)^2} \quad [2]$$

where $MN$ is the total number of data points on the surface, $M$-$h_x$ and $N$-$h_y$ are the number of pairs of data points respectively at a lag distance $h_x \in [-M/2; M/2]$ and $h_y \in [-N/2; N/2]$, $Z_{j,k}$ is the random variable representing the surface heights $z(x, y)$.

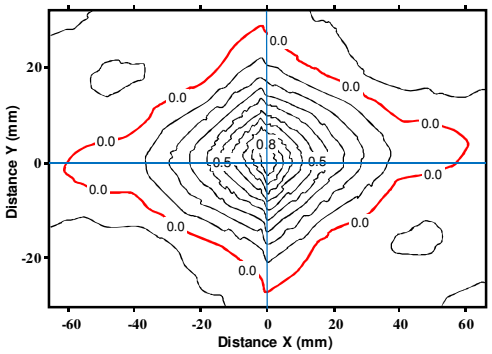


Figure 2. Typical 2D auto-correlogram of a natural granite joint surface showing the null iso-correlation

With map representation the shape of iso-value (iso-variance or iso-correlation) contours involves anisotropy or isotropy at a given scale of observation. An elliptic shape of the contour indicates a mean anisotropy, while a circular shape of the contour indicates a mean isotropy (see Figure 2).

## 2.2 Geostatistical characterisation of real anisotropy

How to use the 2D variogram or the 2D auto-correlogram in order to characterize the structural anisotropy? Which iso-value contour is representative of the whole surface structure? The answer is that for the 2D variogram ("variomap") it is necessary to determine the "range" values in all directions from which the corresponding iso-variance contour is drawn, while for the 2D auto-correlogram, it is sufficient to consider the null iso-correlation contour (see Figure 2). Indeed, one of the essential properties of the auto-correlation function, $\rho(h_{x,y})$, is that the lag at which it becomes null corresponds to the correlation distance $d_c$. Beyond this distance the data are no longer correlated and are therefore random. This property makes possible and easy the direct description of the real structural anisotropy based on the null iso-correlation contour of the 2D auto-correlogram (Eq. 2). The 2D auto-correlogram (or correlomap) is therefore the appropriate tool for the direct characterization of the real structural anisotropy of rock joints (Figure 2).

When the null iso-correlation draws a circle or can be fitted with a circle, the surface presents a structural isotropy. In contrast when this iso-correlation draws an ellipse or can be fitted with an ellipse then the surface presents a structural anisotropy. Figure 3 presents an idealized anisotropy ellipse drawn on a schematic 2D-correlogram.

To characterize the real structural anisotropy of surface using the null iso-correlation, it is suggested to fit it with an ellipse for which the half-major axis $R$ and the half-minor axis $r$ can be calculated as follows (Belem et al. 2000):

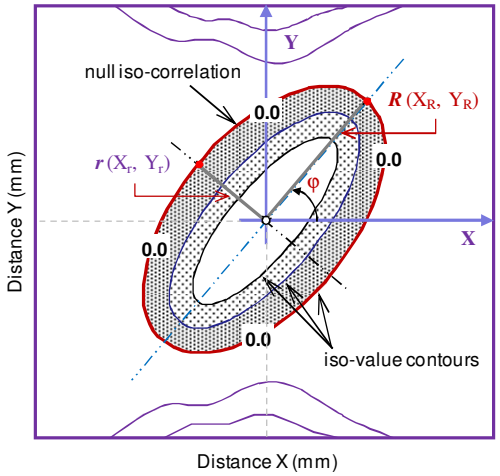


Figure 3. Idealization of anisotropy ellipse based on the 2D auto-correlogram

$$\begin{cases} R = \sqrt{(X_R)^2 + (Y_R)^2} = a \\ r = \sqrt{(X_r)^2 + (Y_r)^2} = b \\ \varphi = \tan^{-1}\left(\dfrac{Y_R}{X_R}\right) \end{cases} \quad [3]$$

where $X_R$ and $Y_R$ are the coordinates of the half-major axis $R$, $X_r$ and $Y_r$ are the coordinates of the half-minor axis $r$, φ is the principal direction of real structural anisotropy of the joint surface (see Figure 3).

## 2.3 Surface angularity parameters

Belem et al. (2000) proposed a parameter that differently quantifies the positive and negative slopes along a roughness profile in order to take into account the shear direction ($\theta_p$, $\theta_{p+}$, $\theta_{p-}$). For evenly spaced data with a constant step $\Delta x$ along the $x$-axis (for instance), the mean angle of the inclinations of the roughness profiles $\theta_p$ ($-90° < \theta_p < 90°$) is given in the discrete form as follows:

$$\theta_p = \tan^{-1}\left(S_p\right) = \tan^{-1}\left(\frac{1}{N_x - 1}\sum_{i=1}^{N_x - 1}\left|\frac{z_{i+1} - z_i}{\Delta x}\right|\right) \quad [4]$$

where $z_i$ is the algebraic values of asperity heights along the roughness profile, $(N_x - 1)$ is the number of intervals used for the slopes calculation, $\Delta x$ is the sampling step along x-axis. An equivalent formula can be derived for $y$-axis.

The mean positive and negative angles of the inclinations of the profile $\theta_{p+}$ and $\theta_{p-}$ ($-90° < \theta_{p+}, \theta_{p-} < 90°$) can be obtained by first calculating the slope increments $\Delta z/\Delta x$ ($x$-axis for instance) along each profile and

secondly calculating the positive and negative mean angles using the following equations (Belem et al. 2000):

$$\theta_{p+} = \tan^{-1}\left(S_{p+}\right) = \tan^{-1}\left(\frac{1}{M_{x+}}\sum_{i=1}^{M_{x+}}\left(\frac{\Delta z}{\Delta x}\right)_i^{+}\right) \quad [5]$$

$$\theta_{p-} = \tan^{-1}\left(S_{p-}\right) = \tan^{-1}\left(\frac{1}{M_{x-}}\sum_{j=1}^{M_{x-}}\left(\frac{\Delta z}{\Delta x}\right)_j^{-}\right) \quad [6]$$

where $M_{x+}$ and $M_{x-}$ are the number of intervals on which are respectively calculated the positive slope $(\Delta z/\Delta x)_+$ and the negative slope $(\Delta z/\Delta x)_-$ increments. However, during the course of cyclic shearing along one direction (*x*- or *y*-axis), and for an interlocked joint, $\theta_{p+}$ will be taken into account in forward direction (for instance) and $\theta_{p-}$ in reverse direction.

The weighted means of Eqs 4–6 over the total number $N_p$ of the entire surface profiles along *k* direction (*k* represents *x*- or *y*-axis) correspond to the "pseudo-surfacial" parameters $(\bar{\theta}_p)_k$, $(\bar{\theta}_{p+})_k$ and $(\bar{\theta}_{p-})_k$ given by the following equations (Belem et al. 2000):

$$\left(\bar{\theta}_p\right)_k = \tan^{-1}\left(\sum_{j=1}^{N_p}\left(S_p\right)_{kj} L_{kj} \Big/ \sum_{j=1}^{N_p} L_{kj}\right) \quad [7]$$

$$\left(\bar{\theta}_{p+}\right)_k = \tan^{-1}\left(\sum_{j=1}^{N_p}\left(S_{p+}\right)_{kj} L_{kj(+)} \Big/ \sum_{j=1}^{N_p} L_{kj(+)}\right) \quad [8]$$

$$\left(\bar{\theta}_{p-}\right)_k = \tan^{-1}\left(\sum_{j=1}^{N_p}\left(S_{p-}\right)_{kj} L_{kj(-)} \Big/ \sum_{j=1}^{N_p} L_{kj(-)}\right) \quad [9]$$

where ($L_{kj} \geq 0$) is the nominal length of the profile along the *k*-axis, $L_{kj(+)} = M_{k+}(\Delta k)$ and $L_{kj(-)} = M_{k-}(\Delta k)$ are the weight factors.

### 2.4 Coefficient of apparent anisotropy of surface

The weighted mean angle $(\bar{\theta}_p)_k$ calculated along the *x*- and *y*-axis using Eq. 7 describes the apparent structural anisotropy of surface morphology with regard to *x* (0° or 180°) and *y* (90° or 270°) directions. The coefficient of apparent anisotropy of surface morphology $k_a$ is defined as the ratio of the half-minor axis ***b*** and the half-major axis ***a*** of apparent anisotropy ellipse and given as follows (Belem et al. 2000):

$$k_a = \frac{b}{a} = \frac{\min\left\{\bar{\theta}_{p(x,y)}\right\}}{\max\left\{\bar{\theta}_{p(x,y)}\right\}} \qquad 0 \leq k_a \leq 1 \quad [10]$$

where subscripts (*x*, *y*) denote the weighted mean angle calculated along the *x*- and *y*-axis.

It was assumed that the direction associated with the $min\{\bar{\theta}_{p(x,y)}\}$ value is close (or corresponds) to the major principal direction of real structural anisotropy of surface. Parameter $k_a$ exclusively quantifies apparent anisotropy with respect to the *x*- and *y*-axis of a test sample. Any deviation from this coordinates system is not taken into account. That is to say $k_a$ is unable to account for the principal direction of real structural anisotropy of the joint surface φ (Eq. 3).

When $k_a = 0$, the surface morphology is perfectly anisotropic (e.g., saw-tooth and corrugated surfaces, etc.); when $k_a = 1$ ($\bar{\theta}_{p(y)} = \bar{\theta}_{p(x)}$) the surface morphology is perfectly isotropic. In addition, if $k_a = \bar{\theta}_{p(y)}/\bar{\theta}_{p(x)}$, the major principal direction of real anisotropy is parallel to *y*-axis (transverse to *x*-axis), while if $k_a = \bar{\theta}_{p(x)}/\bar{\theta}_{p(y)}$, the major principal direction of real anisotropy is parallel to *x*-axis (transverse to *y*-axis). It should be noted that $k_a$ may well be equally calculated using Z2 parameter ($Z2_x$ and $Z2_y$) and the positive or negative angularity parameters defined in Equations 8 or 9.

A real anisotropic surface having a major principal axis oriented at 45° regarding *x*-axis or *y*-axis (see e.g., the lengthening direction of the anisotropy ellipse in Figure 3) gives $k_a = 1$ ($\bar{\theta}_{p(y)} = \bar{\theta}_{p(x)}$) indicating an erroneous isotropic surface. Consequently, the limitations of the $k_a$ parameter make it better suited for the characterization of man-made or numerically generated artificial anisotropic joint surfaces (saw-tooth, corrugated, etc.) because it is insufficient for real structural anisotropy analysis (Belem et al. 2007). In general however, rock joint samples are sheared along the *x* or *y* directions (only multiaxial shearing machines can shear a joint sample along an intermediate direction).

Even if the *x* direction supporting the joint shearing differed from the minor or major principal axis of real structural anisotropy, the semi-quantitative $k_a$ parameter would have no significant impact. Indeed, based on the above assumption, the principal direction of the real anisotropy should be perpendicular to the one fitted to the weighted mean angles $\bar{\theta}_{p(y)}$ and $\bar{\theta}_{p(x)}$ which define $k_a$. Consequently, the apparent anisotropy is related indirectly to the real structural anisotropy of the surface (see Figure 4).

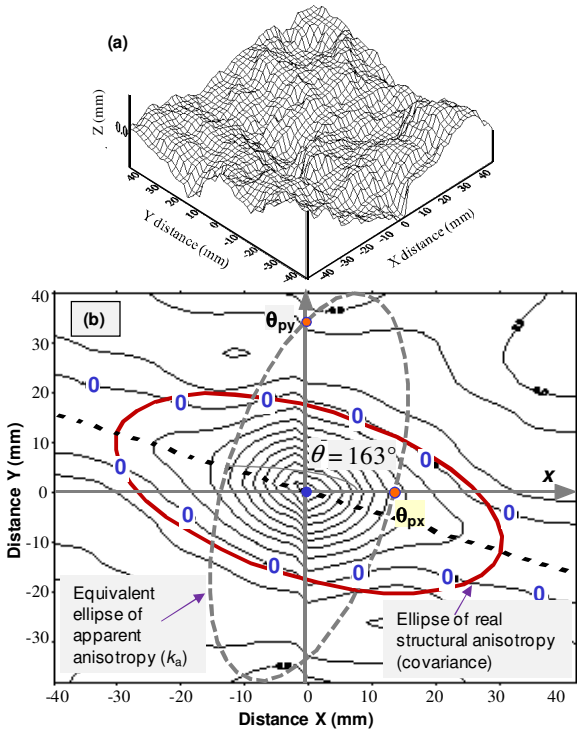


Figure 4. Illustration of the real and apparent anisotropy: a) joint surface, b) 2D auto-correlogram and the ellipses of real and apparent structural anisotropy

Apparent structural anisotropy of surface morphology was arbitrarily subdivided into four classes: class I, II, III and IV. Table 1 presents the range of variation of $k_a$ for the fourth classes and Figure 5 illustrates these fourth classes and their description.

Table 1. Classification of apparent anisotropy of surface

| Class of anisotropy | Range of $k_a$ | Description |
|---|---|---|
| Class I | $0 \le k_a < 0.25$ | Anisotropic |
| Class II | $0.25 \le k_a < 0.5$ | Moderately anisotropic |
| Class III | $0.5 \le k_a < 0.75$ | Moderately isotropic |
| Class IV | $0.75 \le k_a \le 1$ | Isotropic |

## 3 NEW APPROACH OF CHARACTERIZATION OF PRIMARY ROUGHNESS

### 3.1 Degree of apparent anisotropy of surface

The easiest way to quantify the apparent anisotropy of surface is to have a parameter which value will be zero when the surface is not anisotropic (i.e. isotropic) and 1 when the surface is perfectly anisotropic. From the already defined coefficient of apparent anisotropy $k_a$, the degree of apparent anisotropy $\delta_a$ can be defined as follows:

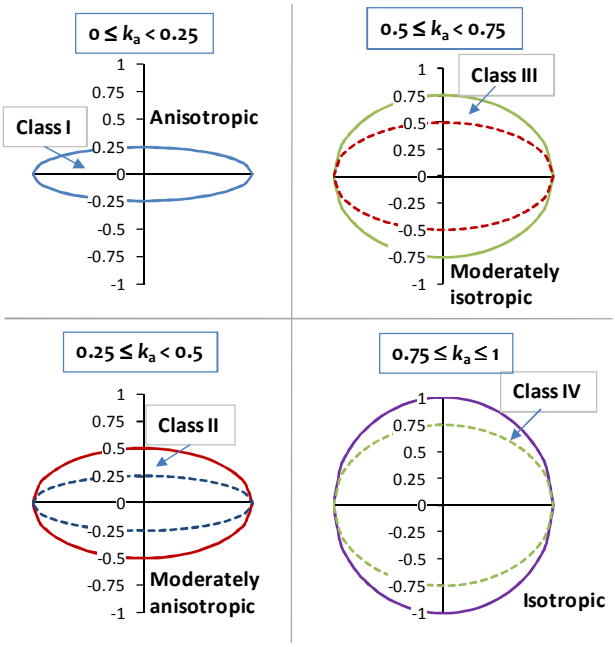


Figure 5. Schematic illustration of apparent anisotropy ellipses based on $k_a$ values

$$\delta_a = 1 - k_a \qquad 0 \le \delta_a \le 1 \qquad [11]$$

### 3.2 Degree of real structural anisotropy of surface

The principal direction of real structural anisotropy φ corresponds to the direction of the lengthening of the ellipse and therefore to the mean direction of the surface geometric texture (see Figures 3 and 4b). Considering for example a corrugated surface, that results in the fact that this principal direction φ is on average parallel to the orientation of the peaks of the undulations. For such surfaces, it's therefore expected to have higher values of angularity parameters along the transverse direction to the principal direction of anisotropy (Figure 4b). It should be emphasized that the 2D auto-correlogram highlights the spatial organization of the structures forming the geometry of surface, while the angularity parameters describes the geometry of the asperities.

From Figure 3 and Equation 3, the half-major axis $R$ and the half-minor axis $r$ can be used to define the degree of real structural anisotropy of surface $\delta_r$ which is given as follows:

$$\delta_r = \frac{R-r}{r} = \frac{\sqrt{X_R^2 + Y_R^2}}{\sqrt{X_r^2 + Y_r^2}} - 1 = \frac{R}{r} - 1 \qquad 0 \le \delta_r \le \delta_{r\_\max} \qquad [12]$$

When $\delta_r = 0$ the ellipse is reduced to a circle ($R = r$) and the surface is no longer anisotropic but rather

perfectly isotropic. The surface start to exhibit anisotropic structure from $\delta_r = 1$ ($R = 2r$) to $\delta_r = \delta_{r\_max}$ ($R > 2r$). It is clear that $\delta_{r\_max}$ value depends on the ellipse axis ratio which may be as high as 6 ($R = 6r$). When the surface is anisotropic, the principal direction of real structural anisotropy of the joint surface φ is given by Eq. 3.

### 3.3 Alternative definition of the degree of real structural anisotropy of surface

Even if the method of fitting an ellipse of anisotropy to the null iso-correlation is rigorous and relevant, it remains mostly manual and laborious. Indeed, the user must first obtain the autocorrelation map (using for example the commercial software Surfer®) and then manually fit the ellipse to the null iso-correlation.

That is why it is desirable to find an alternative method of direct calculation of $\delta_r$. Indeed, one could use polar sections spaced at constant angle across the 2D auto-correlogram to obtain different 1D correlograms in these directions (Figure 6a). From these polar sections, when the surface is structurally isotropic, all 1D correlograms must give a single value of correlation distance $d_c$. On the contrary, if the surface is anisotropic different values of $d_c$ must be obtained and consequently lower and upper limits can be found: $d_{c\_min}$ and $d_{c\_max}$. From Figure 6b and the known upper ($d_{c\_max}$) and lower ($d_{c\_min}$) limits of the correlation distance $d_c$, the degree of real structural anisotropy of surface can be defined as follows:

$$\delta_r = \frac{d_{c\_max} - d_{c\_min}}{d_{c\_min}} = \frac{d_{c\_max}}{d_{c\_min}} - 1 \qquad 0 \le \delta_r \le \delta_{r\_max} \qquad [13]$$

In Eq. 13, when $\delta_r = 0$ ($d_{c\_max} = d_{c\_min} = d_c$) the joint surface is perfectly isotropic. When $\delta_r = 1$ the surface starts to become anisotropic and $d_{c\_max} = 2d_{c\_min}$. This version of $\delta_r$ is easier to calculate than the one given by Eq. 12.

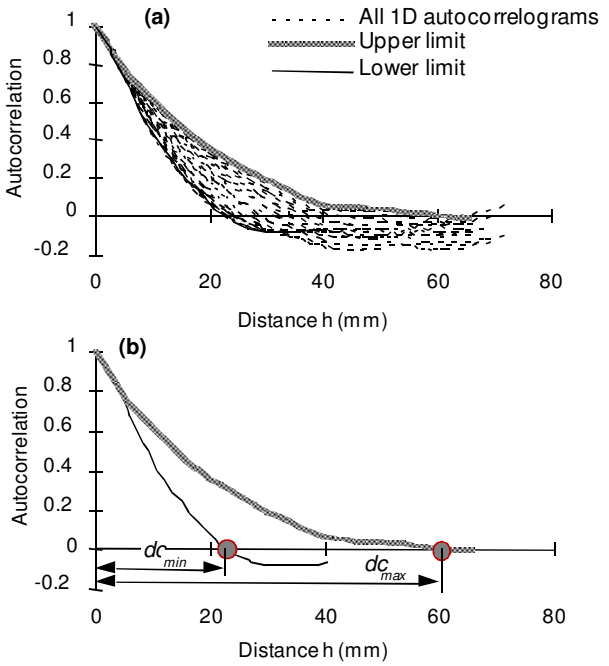


Figure 6. 1D correlogram: a) all the polar section profiles, b) lower and upper limit of the correlation distance $d_c$

### 3.4 Anisotropy function

Generally, the calculation of various 2D parameters is done only with regard to *x*- and *y*-axis. Therefore, it would be interesting to predict the value of these parameters for any direction φ. Such an approach has already been adopted by Aydan et al. (1996) which proposed an anisotropy function without any link to an ellipse of anisotropy. These authors have proposed a general anisotropy function $F(\varphi)$ for predicting the angularity parameters of any type of surface anisotropy in any direction φ which is given as follows:

$$F(\varphi) = a_1 \cos\varphi + b_1 \sin\varphi + a_2 \cos^2\varphi + b_2 \sin^2\varphi \qquad [14]$$

where $a_1 = (F_{0°} - F_{180°})/2$, $b_1 = (F_{90°} - F_{270°})/2$, $a_2 = (F_{0°} + F_{180°})/2$, $b_2 = (F_{90°} + F_{270°})/2$. Constants $a_1$ and $b_1$ will always vanished for angularity parameters not taking into account positive and negative angles.

An equivalent anisotropy function was earlier proposed by Wong (1985) and is given as follows:

$$Z(\varphi) = Z_{0°} + (Z_{90°} - Z_{0°}) \sin^2\varphi \qquad [15]$$

Even if we could be satisfied with these two functions, its remains that they have not been defined taking into account the ellipse of surface anisotropy. As previously argued, it is clear that real structural anisotropy can be well described by an ellipse of anisotropy. Knowing the three parameters describing this ellipse (half-major axis

*R*, half-minor axis *r* and the principal direction of anisotropy φ) it can be interesting to express or calibrate the weighted mean angularity parameters $\bar{\theta}_{p(x)}$ (= $P_x$ = $P_{0°/180°}$) and $\bar{\theta}_{p(y)}$ (= $P_y$ = $P_{90°/270°}$) with the ellipse of structural anisotropy of surface.

Let $E_1$ be the ellipse of real structural anisotropy of surface determined from 2D autocorrelogram. Assuming that the principal direction associated with $min\{\bar{\theta}_{p(x,y)}\}$ is in "average" to the principal direction of real anisotropy surface, it is considered that the ellipse of apparent anisotropy of surface $E_2$ for 2D geometric parameters is perpendicular to $E_1$. The calibration of 2D geometric parameters can be done on the ellipse of apparent anisotropy from which the value of each geometric parameter *P* along any direction φ can be obtained using a new anisotropy function *P*(φ). The initial parameters $P_x$ and $P_y$ correspond to the ones calculated with respect to the *x*-axis (φ = 0° or 180°) and *y*-axis (φ = 90° or 270°), that is to say $P_x = P_{0°/180°}$ and $P_y = P_{90°/270°}$. The general form of the anisotropy function is given as follows:

$$P(\varphi) = \sqrt{\left(P_{0°/180°}\cos^2\varphi\right)^2 + \left(P_{90°/270°}\sin^2\varphi\right)^2} \qquad [16]$$

Note that this equation gives results similar to those obtained using Equations 14 and 15. Figure 7 presents a comparison of these three anisotropic functions. When the joint surface is isotropic or nearly isotropic, the three functions are identical (Figure 7a). On the contrary, for anisotropic surfaces the proposed Eq. 16 gives higher values than Eqs. 14 and 15 (see Figure 7b & c). We believe that this difference is mainly due to the fact that Eq. 16 explicitly takes into account the ellipse of structural anisotropy of surface and its size on the angularity parameters (unlike the Equations 14 and 15).

### 3.5 Coefficient of geometric irregularity of surface

The positive and negative weighted mean angles can also assess the degree of irregularity of surface $g_i$ in a direction *k* (*x* or *y*). Indeed, the parameter $g_i$ is defined as the ratio of the weighted mean angle $(\bar{\theta}_{p+})_k$ and the weighted mean absolute value of $(\bar{\theta}_{p-})_k$ which quantifies the degree of geometric irregularity of the surface along *x, y* or in the *xy* plan and is given as follows:

$$g_i = \frac{\left(\bar{\theta}_{p+}\right)_{x,y}}{\left(\left|\bar{\theta}_{p-}\right|\right)_{x,y}} \quad \text{with} \quad 0 < g_i \le g_{i_{max}} \qquad [17]$$

$$g_i = \frac{\left(\bar{\theta}_{p+}\right)_x + \left(\bar{\theta}_{p+}\right)_y}{\left(\left|\bar{\theta}_{p-}\right|\right)_x + \left(\left|\bar{\theta}_{p-}\right|\right)_y} \quad \text{with} \quad 0 < g_i \le g_{i_{max}} \qquad [18]$$

When $g_i$ = 1, the surface is perfectly regular (regular triangles, sinusoids, circular sections, etc.); when 0 < $g_i$ < 1 the surface is irregular with an average maximum mean negative angle, and when 1 < $g_i$ ≤ $g_{i\_max}$ the surface is irregular with an average maximum mean positive angle (Figure 8). Although at first glance this parameter seems to not present a great interest because of its simplicity, it can allow classifying anisotropic irregular surfaces by distinguishing them better. For regular surface the fractal dimension is a better parameter than the degree of irregularity.

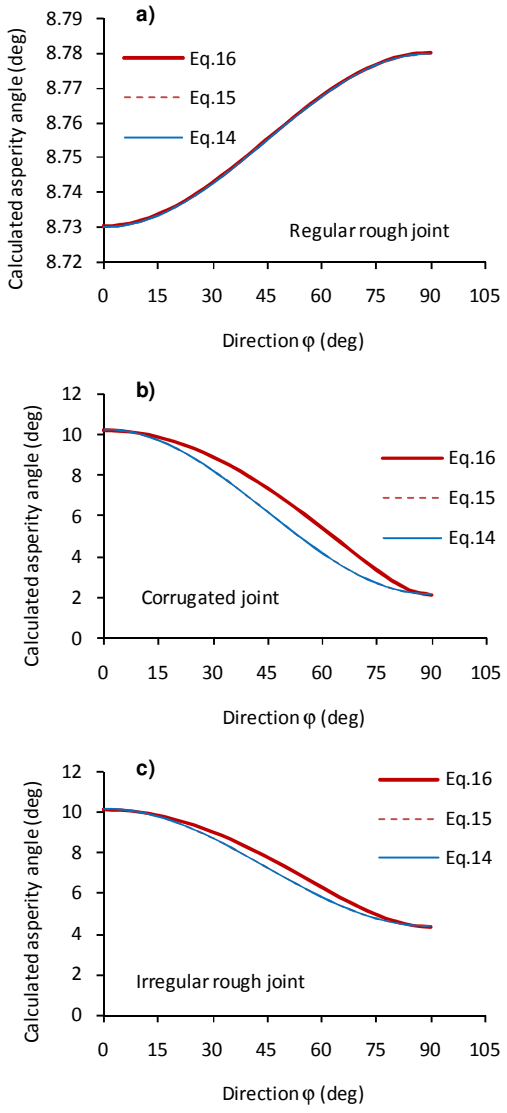


Figure 7. Comparison of predicted weighted mean angles using the three anisotropy functions and for three different joint surfaces

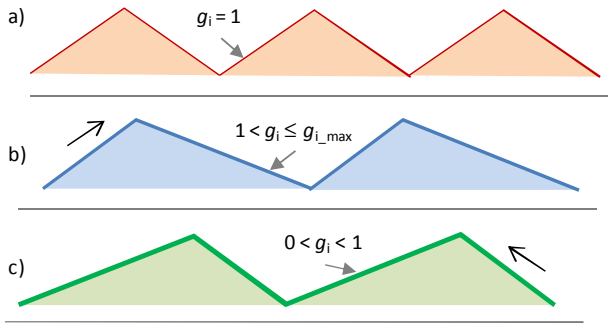


Figure 8. Schematic illustration of 2D geometric irregularity of surface along one direction

### 3.6 Degree of surface waviness

An undulating surface can be fully described by its maximum amplitude $a_m$, $\lambda_x$ the wavelength or period along the *x*-axis and $\lambda_y$ the wavelength or period along the *y*-axis (see Figure 9). From Figure 9 we define the degree of surface waviness which is given as follows:

$$W_s = \frac{2\alpha}{\pi} = \frac{2}{\pi}\tan^{-1}\left(\frac{4a_m}{\lambda_{x,y}}\right) \quad \text{with} \quad 0 \leq W_s < 1 \qquad [19]$$

Equation 19 shows that when $W_s = 0$ the surface is perfectly flat and smooth and therefore non-corrugated. When $W_s$ tends towards 1 the surface undulations look like "needles" or sticks. A parametric study has shown that for a perfectly isotropic surface, the autocorrelation distance $d_c \approx \lambda_{x,y}/2$, while for anisotropic surfaces, $d_c \approx \lambda_{x,y}/4$.

Even if this parameter is intended for anisotropic corrugated surfaces, it can still be used for all surfaces. In that case, the waviness is viewed in average.

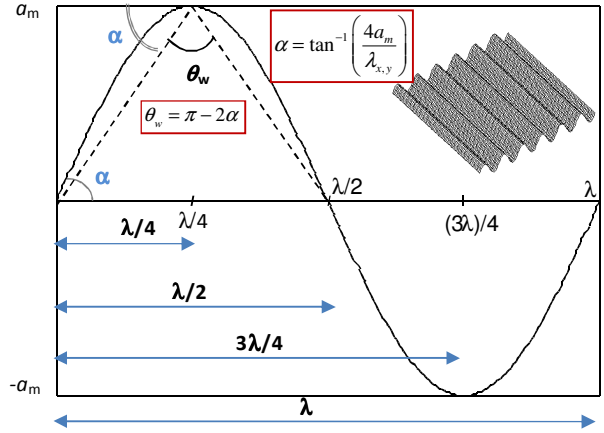


Figure 9. Parameters describing a sinusoid linear profile of one wavelength

## 4 CONCLUSION

In this study, numerous parameters have been proposed for the quantitative characterization of the primary roughness of rock joint surfaces. These parameters include the degrees of apparent and real anisotropy of surface, the coefficients of real anisotropy and geometrical irregularity, the anisotropy function and the degree of waviness. The calculations of these parameters rely primarily on 3D analysis of surface topography data. Since new laser tools such as LiDAR have been developed for the scanning of field scale fracture surfaces, this implies that the proposed parameters are widely applicable at large scale.


## ACKNOWLEDGEMENTS

This research was partly supported by the Fond de la Fondation de l'UQAT FUQAT and the NSERC Discovery Grant Program. The authors gratefully acknowledge their support.


## REFERENCES


Aydan, Ö., Shimizu, Y. and Kawamoto, T. 1996. The anisotropy of surface morphology characteristics of rock discontinuities. *Rock Mech. & Rock Engng.* 29(1):47-59.

Belem, T., Souley, M., Homand, F. 2007. Modelling rock joint walls surface degradation during monotonic and cyclic shearing. *Acta Geotechnica*, 2: 227–248.

Belem, T., Homand-Etienne, F. and Souley, M. 2000. Quantitative Parameters for Rock Joint Surface Roughness. *Rock Mech. Rock Engng.* 33(4): 217–242.

Fardin, N. 2008. Influence of Structural Non-Stationarity of Surface Roughness on Morphological Characterization and Mechanical Deformation of Rock Joints. *Rock Mech. Rock Engng.* 41(2): 267-297.

Fardin, N, Stephansson, O. and Jing, L. 2001. The scale dependence of rock joint surface roughness. *Int J Rock Mech Min Sci* 38: 659–669.

Feng, Q., Fardin, N., Jing, L. and Stephansson, O. 2003. A New Method for In-situ Non-contact Roughness Measurement of Large Rock Fracture Surfaces. *Rock Mech Rock Engng.* 36(1): 3–25.

Grasselli, G. 2006. Manuel Rocha Medal Recipient – Shear Strength of Rock Joints Based on Quantified Surface Description. *Rock Mech Rock Engng.* 39 (4): 295–314.

Jing. L. 2003. A review of techniques, advances and outstanding issues in numerical modelling for rock mechanics and rock engineering. *Int J Rock Mech Min Sci* 40: 283–353.

Journel, A. 1975. *Géostatistique minière*. Centre de Géostatistique de Fontainbleau, Paris, France.

Kana, D.D., Fox, D.J. and Hisiung, S.M. 1996. Interlock/friction model for dynamic shear response in natural jointed rock. *Int. J. Rock Mech. Min. Sci. & Geomech. Abstr.*, 33(4): 371-386.

Lato, M, Hutchinson., D.J., Diederichs, M.S. and Harrap, R. 2009. Optimization of LiDAR scanning and processing for automated structural evaluation of discontinuities in rockmasses. *Int J Rock Mech Min Sci* 46: 194–199

Lato, M., Hutchinson, J., Diederichs, M. and Kalenchuk, K. 2007. Evaluating block shape and block volume distributions of rock faces using LiDAR and 3DEC. *Geophys Res Abstr* (European Geosciences Union) 9: 1–2

Rasouli, V. and Harrison, J.P. 2000. Scale effect, anisotropy and directionality of discontinuity surface roughness. *Proc., EUROCK 2000*. Nationales Symposium für Felsmechanik und Tunnelbau, Aachen, Germany, 751–756

Renard, F., Voisin, C., Marsan, D. and Schmittbuhl, J. 2006. High resolution 3D laser scanner measurements of a strike-slip fault quantify its morphological anisotropy at all scales: *Geophysical Research Letters*, 33, (L04305), doi: 10.1029/2005GL025038.

Sagy, A., Brodsky, E.E. and Axen, G.J. 2007. Evolution of fault-surface roughness with slip. *Geology*, 35(3): 283–286.

Sharifzadeh, M., Mitani, Y. and Esaki, T. 2006. Rock Joint Surfaces Measurement and Analysis of Aperture Distribution under Different Normal and Shear Loading using GIS. *Rock Mech. Rock Engng.*, 41(2): 299-323.

Wong, T. F. 1985. Geometric probability approach to the characterization and analysis of microcracking in rocks. *Mechanics of Materials*, n°4, pp.261-276.